ARCHIVES OF ELECTRICAL ENGINEERING VOL. 64(3), pp. 471-486 (2015)

DOI 10.2478/aee-2015-0036

Steady-state time-periodic finite element analysis of a brushless DC motor drive considering motion

MARIUSZ JAGIEŁA, JANUSZ GWOŹDŹ

Opole University of Technology
Institute of Electromechanical Systems and Industrial Electronics
ul. Prószkowska 76, 45-758 Opole, Poland
e-mail: m.jagiela@po.opole.pl, j.gwozdz@doktorant.po.edu.pl

(Received: 02.12.2014, revised: 16.04.2015)

Abstract: This paper aims at providing a framework for comprehensive steady-state time-domain analysis of rotating machines considering motion. The steady-state waveforms of electromagnetic and circuit quantities are computed via iterative solution of the nonlinear field-circuit-and-motion problem with constraints of time periodicity. The cases with forced speed and forced load torque are considered. A comparison of execution times with a conventional time-stepping transient model is carried out for two different machines. The numerical stability of a time-periodic model with forced speed is shown to be worse than that of traditional transient time-stepping one, although the model converges within a reasonable number of iterations. This is not the case if forced load via equation of mechanical balance is accounted for. To ensure convergence of the iterative process the physical equation of motion is replaced by the fixed-point equation. In this way the model delivers time-periodic solutions regarding not only the electromagnetic quantities but also the rotational speed.

Key words: finite elements, brushless machines, inverter drives, steady-state, mathematical modeling

1. Introduction

A considerable execution time of the transient time-stepping finite element models of electrical machines is a generally accepted tradeoff between the computational cost and accuracy. For determination of the performance characteristics it would be, however advantageous to be able to restrict analysis to the steady-state. Often, the quasi-stationary "frame of reference" models are used with this purpose [1-5]. For some machines, such as motors driven from quasi-square voltage wave inverters, such an analysis can be too approximate.

For more accurate modeling it is necessary to use models that do not restrict the type of time variations of variables or excitations. There are two comprehensive approaches that match this requirement. The first of them is the harmonic balance finite element method

(HBFEM) [6, 7], and the second one is based on the formulation of the time-dependent problem using constraints of time periodicity, known as the time-periodic finite element method (TPFEM) [8-13]. The HBFEM is recognized as being competitive with the transient time-stepping model with respect to the execution time [7], although its accuracy may be limited when considering nonlinearity or high ordinals of time harmonics (switched currents). The latter method, advocated in this paper, considers the domain of time as the fourth dimension onto which the periodicity constraints are imposed. The basic TPFEM gathers equations for all time-steps in a particular nonsymmetric system of equations, and consequently, it requires extensive computations and suitable solvers. There are a few implementations of this method, which make it more cost-effective, namely: the explicit error correction methods [11] or parallelization [12, 14]. Currently, there are the system-level simulators available whose functionality includes the ability to predict the steady-state waveforms in switched circuits using this method [15], yet this is not the case in the state-of-the-art finite element analysis systems.
In this work, we use the time-periodic model in an analysis of a permanent magnet brushless DC (BLDC) motor driven from a power converter with commutation feedback, taking account for nonlinearity, stack skew and motion. The two cases are distinguished with respect to how the mechanical motion can be accounted for in this type of model, namely:

- prescription of constant angular speed to the rotor and constraining the time-step size;
- calculation of angular speed as a time-periodic waveform using the equation of mechanical balance.

Use of the second case has some practical implications, and to the best of our knowledge, such a model has not been proposed so far. An extension of this work beyond our previous research [16] is a proposal of the TPFEM algorithm for cases where the equation of mechanical balance is taken into account. In the two aforementioned approaches the steady-state waveforms are determined via iterative solution of a nonlinear problem, but their numerical features are different, and this is reported in the following.

2. Time-periodic model of BLDC motor

2.1. Basic equations

Consider a BLDC motor drive comprised of a three-phase machine and a symmetric two-level voltage source inverter, as shown in Figure 1a. The inverter is to be represented by the circuit network containing linear (R_s, L_s, R_f, C_f), nonlinear (parallel diodes) and two-state (transistors) elements (see Fig. 1b). To represent a rudimentary behavior of switching elements, particularly so as to allow for modeling the commutation effects, the inductances L_t and L_d are added in series with resistors. The nonlinear resistance of the diode is calculated from the static characteristic, whilst the resistance of the transistor varies between a small value during the turn-on state and a high value during the turn-off state.

Although the system containing explicit models of semiconducting elements could be considered unjustified in other types of machines, here it is the only correct approach to handle the “spiky” waveforms of phase voltages and the energy return process through parallel

diodes for various conditions of operation. It should be noticed that such a model is sufficiently accurate to account for the conduction losses as well as the global commutation effects, it is however too approximate to represent the high-frequency operation of semiconducting elements.

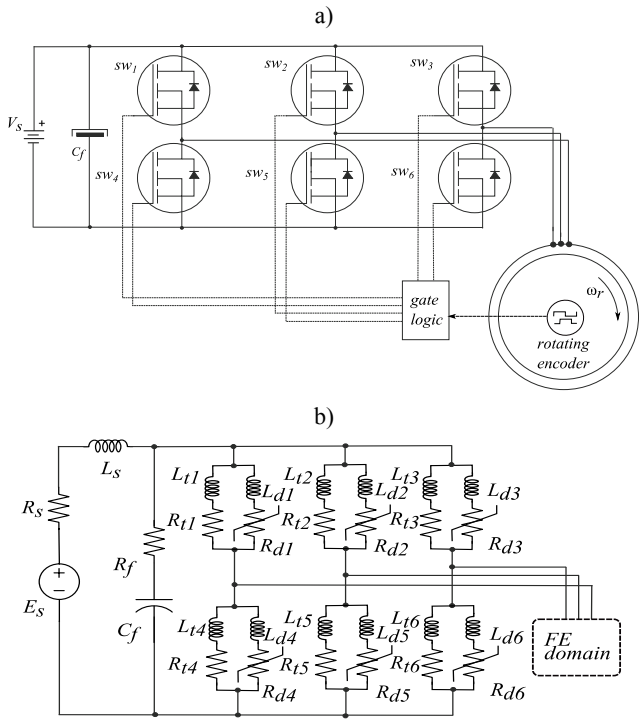

Fig. 1. Drive system for permanent magnet BLDC motor: a) overall diagram, b) functional circuit model of voltage source inverter

The motor itself is modelled considering a two-dimensional distribution of the magnetic field over the axially distributed mesh slices to approximate the stator stack skew (2.5-D model) [18, 19]. Equations that result from the discrete approximation of the Ampere's law, and those fulfilling the Kirchhoff's laws in the electric circuits can be written in the form:

$$[S(\varphi)][\varphi]+[G]\frac{d}{dt}[\varphi]-[F(\varphi)]-[K_1]i-[B^T][\lambda]=0, \tag{1}$$

$$\frac{\ell[K_1^T]}{n_S}\frac{d}{dt}[\varphi]+L\frac{d}{dt}i+Ri+K_2^T u_C=V, \tag{2}$$

$$K_2 i-C_f\frac{d}{dt}u_C=0. \tag{3}$$

These equations are supplemented by constraints involving the homogeneous Dirichlet boundary condition imposed on the motor outer frame, periodic conditions imposed on the parallel lines of symmetry with respect to one pole-pair, and the field continuity conditions imposed at the sliding interface between stator and rotor so as to allow for mesh rotation. These are to be written in the form:

$$[B][\varphi] = [0]. \tag{4}$$

The initial conditions for the ordinary differential equations in (1)-(3) are:

$$\begin{aligned} &[\varphi(t=0)] = [\varphi_0], \\ &i(t=0) = 0, \\ &u_C(t=0) = u_{C0}. \end{aligned} \tag{5}$$

In (1)-(5) $[\varphi]$ is the vector of nodal values of the magnetic vector potential, $[\varphi]$ the vector of its initial values obtained from a single solution of the magnetostatic problem at $t = -\infty$, t the vector of currents, u_C the voltage across the capacitor with u_{C0} being its initial value, $[S]$ the reluctance matrix, $[G]$ the conductance matrix, $[F]$ the vector of currents due to permanent magnets' mmf, and $[\lambda]$ is the vector of surface currents attributed to the Lagrange multipliers used to conveniently handle the boundary and interface conditions. The field equation (1) is coupled with circuit equations via the winding function matrix $[K_1]$, whilst L and R are the matrices of circuit inductances and circuit resistances, respectively, $[K_2]$ is the auxiliary matrix, and V is the vector of voltage sources. The square brackets denote block matrices and block vectors that result from the approximation of a stator stack skew by the axially distributed mesh slices, and ℓ and n_S are the machine length and number of mesh slices, respectively. There are a few ways to derive the matrices in Equation (1) depending on the discretization method used [20], that will not be discussed here. The above system of equations describes the machine in transient conditions. In order to obtain the steady-state solution one needs to solve it within the range of time being a few times larger than the largest time-constant. On the contrary, in the time-periodic models, it is stated that a condition for the steady-state in (1)-(4) is to fulfill the constraint equations:

$$\begin{aligned} &[\varphi(t=t_1)] = [q_\varphi][\varphi(t=t_1+T)], \\ &[\lambda(t=t_1)] = [q_\lambda][\lambda(t=t_1+T)], \\ &i(t=t_1) = q_i i(t=t_1+T), \\ &u_C(t=t_1) = q_u u_C(t=t_1+T), \end{aligned} \tag{6}$$

where t_1 is the instant of time and T is the time-period equal to the largest fundamental period or half of it. The matrix operators $[q_\varphi]$, q_i and q_u are used to match the variables in both cases. In the first case, these are the identity matrices, which means that the value and sign of each variable at time $t = t_1$ equals the value and sign of the same variable at $t = t_1 + T$. In the inverter-driven machine this is not the case when T equals one half period. In such a situation some variables, such as the DC-link current, and capacitor voltage and current, experience

positive periodicity, some other ones, such as phase currents and nodal magnetic potentials experience negative periodicity, and yet some, such as the transistor and diode currents need to be cross-coupled. Taking (6) as the constraints imposed on (1)-(4), the initial value problem is transformed into the boundary value problem with periodic conditions. Discretization of the time domain is carried out using the backward Euler method. Assuming that T is subdivided into m-1 time intervals equal to Δt, there are m points in which the solution has to be obtained, thus for k = 1, 2, ..., m, from (1)-(4) we get:

$$\begin{bmatrix} [S_k]+\dfrac{[G_k]}{\Delta t} & [\mathrm{B}^{\mathrm{T}}] & [\mathrm{K}_1] & 0 \\ [B] & 0 & 0 & 0 \\ \dfrac{\ell[K_1^T]}{n_s\Delta t} & 0 & \mathrm{R_k}+\dfrac{L}{\Delta t} & K_2^T \\ 0 & 0 & -\mathrm{K}_2 & \dfrac{c_f}{\Delta t} \end{bmatrix} \begin{bmatrix} \varphi_k \\ \lambda_k \\ i_k \\ u_{ck} \end{bmatrix} - \begin{bmatrix} \dfrac{[G_{k-1}]}{\Delta t} & 0 & 0 & 0 \\ 0 & 0 & 0 & 0 \\ \dfrac{\ell[K_1^T]}{n_s\Delta t} & 0 & \dfrac{L}{\Delta t} & 0 \\ 0 & 0 & 0 & \dfrac{c_f}{\Delta t} \end{bmatrix} \begin{bmatrix} \varphi_{k-1} \\ \lambda_{k-1} \\ i_{k-1} \\ u_{c(k-1)} \end{bmatrix} = \begin{bmatrix} [0] \\ [0] \\ V_{k-1} \\ 0 \end{bmatrix}, \quad (7a)$$

while from (6):

$$diag\left([q_\varphi],[q_\lambda],q_i,q_u\right) \begin{bmatrix} \varphi_m \\ \lambda_m \\ i_m \\ u_{cm} \end{bmatrix} = \begin{bmatrix} \varphi_0 \\ \lambda_0 \\ i_0 \\ u_{c0} \end{bmatrix}, \quad (7b)$$

For the simplicity of considerations we will use a more compact notation for (7):

$$D_1x_1 - E_0Q_sx_m = H_0 \quad \text{for} \quad k=1 \quad (8a)$$

while:

$$D_kx_k - E_{k-1}x_{k-1} = H_{k-1} \quad \text{for} \quad k=2, ..., m \quad (8b)$$

With $Q_s = diag([q_\varphi],[q_\lambda],q_i,q_u)$ and $x_k = [[\varphi_k]\ [\lambda_k]\ i_k\ \ u_{ck}]^T$. If there are n_u unknowns in each k-th subsystem in (8), then it becomes a system of $n_u{\cdot}m$ equations to be solved simultaneously. It is worth noticing that the application of the backward Euler method makes this problem solvable due to a radically reduced number of nonzero entries in E_{k-1} and the ensured L-stability of the difference equations of stiff type. This system is nonlinear due to magnetization characteristics of the magnetic materials and static characteristics of the parallel diodes. The nonlinear equations will be solved via the Newton-Raphson method, where a contribution to the k-th block-row of the Jacobian matrix is:

$$J_1 = D_1 + \left.\frac{\partial D_1}{\partial x_1}\right|_{x_1} x_1 + E_0 + \left(\left.\frac{\partial E_0}{\partial x_0}\right|_{Q_S x_m}\right) Q_S x_m \quad \text{for} \quad k=1 \quad (9a)$$

and

$$J_k = D_k + \left.\frac{\partial D_k}{\partial x_k}\right|_{x_k} x_k + E_{k-1} + \left(\left.\frac{\partial E_{k-1}}{\partial x_{k-1}}\right|_{x_{k-1}}\right) x_{k-1} \quad \text{for} \quad k = 2, ..., m. \tag{9b}$$

Besides lack of symmetry of the Jacobian matrix [9-13], due to application of the Lagrange multipliers, it becomes an indefinite matrix. A crucial problem in making this model competitive to the transient one (with respect to the execution time), is a choice of an efficient solver of this system of linear equations. In this work, we use the UMFPACK package which implements a direct multifrontal solver designated to problems with nonsymmetric matrices that performs well on indefinite problems and takes advantage of a multicore computer architecture [17].

2.2. Motion

Modeling an unconstrained angular movement is carried out by applying interpolation relationships to the entries of [*B*] that correspond with the values of $[\varphi_k]$ connected to a sliding interface between the nonconforming meshes. As a consequence of angular movement these entries, and thus the matrix [*B*], become time-dependent.

2.2.1. Case with prescribed speed and unknown load torque

This approach can be used in determination of the machine characteristics vs. speed. When (8) is solved at the prescribed speed ω_{rp}, in order to obtain a time-periodic solution in *m* points for a machine having *p* pairs of poles, the time-step size has to be constrained by:

$$\Delta t = \frac{2\pi}{p\omega_{rp}(m-1)}. \tag{10}$$

2.2.2. Case with prescribed load torque and unknown speed

Some additional considerations should be involved if the determination of the rotational speed for the given load torque is regarded. Using the model from the previous section this would require the knowledge of average torque around the operation point, and then application of a separate search for speed. Because the location of the machine operation point is not known in advance, one would need to determine almost a complete speed vs. torque characteristic prior to searching for speed, and this would be a costly task. Potentially, a more efficient approach would be to determine the speed directly from the time-periodic model avoiding the need to determine the other points of the characteristic. This is related with a more general case when the load is imposed as a load torque vs. speed curve, although the following considerations will be carried out for the case with constant load torque.

To account for time-varying speed it is necessary to add the equation of mechanical balance to (8), which is to be considered in typical form:

$$I\frac{d\omega_r}{dt} = T_e - T_l - k_f\omega_r, \tag{11a}$$

with a time-periodic condition:

$$\omega_r(t = t_1) = q_{\omega_r}\omega_r(t = t_1 + T), \tag{11b}$$

where I is the moment of inertia, T_e the electromagnetic torque, T_l the load torque, k_f the friction constant and $q_{\omega r}$ the unity matching operator. The periodicity of the rotation angle α_r, required for calculation of the commutation points, is different from those of the other variables. This angle can be calculated from:

$$\frac{d\alpha_r}{dt} = \omega_r \tag{11c}$$

and the periodicity condition is:

$$\alpha_r(t = t_1) = \alpha_r(t = t_1 + T) + q_\alpha \frac{2\pi}{p} \tag{11d}$$

with $q_\alpha = -1$ for a clockwise, and $q_\alpha = 1$ for a counterclockwise direction, respectively. Note that for the given form of (11a), equation (11d) is satisfied perfectly by constraining onlyω_r, and consequently, α_r does not have to be considered as an unknown in (8).

Using the backward Euler formula to dicretize (11a-b), one obtains the difference equation:

$$\omega_{r1}\left(\frac{I}{\Delta t} + k_f\right) - T_{e1}([\varphi_1], [\lambda_1]) = q_{\omega_r}\omega_{rm}\frac{I}{\Delta t} - T_{l0} \quad \text{for} \quad k = 1, \tag{12a}$$

and

$$\omega_{rk}\left(\frac{I}{\Delta t} + k_f\right) - T_{ek}([\varphi_k], [\lambda_k]) = \omega_{r(k-1)}\frac{I}{\Delta t} - T_{l(k-1)} \quad \text{for} \quad k = 2, \ldots, m. \tag{12b}$$

In order to provide the unconditional stability of (12) the electromagnetic torque T_{ek} is calculated implicitly via auxiliary matrix forms [21] using the vectors $[\varphi_k]$ and $[\lambda_k]$, that approximate the Maxwell stress tensor, such that $T_{ek} = [C][\varphi_k^T][\lambda_k] \approx \ell r_a^2 \phi_{l_\psi} B_r H_\psi d\psi$, with $[C]$ being the auxiliary matrix, r_a the average air-gap radius and, and B_r and H_ψ the radial air-gap magnetic flux density and tangential air-gap magnetic field, respectively, and ψ the angular coordinate. In this case the time-step size is dependent on the speed waveform determined from (12), and is to be calculated as:

$$\Delta t = \frac{2\pi}{\frac{p(m-1)}{T}\int_{t_1}^{t_1+T}\omega_r dt}. \tag{13}$$

This creates a very particular algorithm with the time-step size updated in every nonlinear iteration.

When (12) is added to (8) the augmented system is to be solved for $x_k = [[\varphi_k]\ [\lambda_k]\ i_k\ \ u_{ck}\ \ \omega_{rk}]^T$, with $Q_s = diag([q_\varphi], [q_\lambda], q_i, q_u, q_{\omega_r})$, . Once the waveform of angular speed is obtained from (8), the rotation angle required for detection of the commutation zone can be calculated from:

$$\alpha_{rk} = \alpha_{r(k-1)} + \Delta t\omega_k \quad for \quad k = 1, \ldots, m \tag{14}$$

assuming for $k = 1$ initial value α_0 which corresponds to initial rotor position.

With Equation (12) considered, the Jacobian matrix obtains the two important features which need to be discussed. The first one is its singularity if $k_f = 0$, whilst in the transient time-stepping model it would still be unique in a such case. The singularity is due to two identical rows in $\boldsymbol{D}_k$ when a positive time-periodicity on angular speed is imposed ($q_{\omega r} = 1$). This means that equation (12) with positive periodic condition has in this case only the trivial solutions. The second feature regards a very high sensivity of some entries to variations in ω_r, and so in Δt (which is being updated in each iteration acording to (13)). Because the value of the moment of inertia in physical motors is usually a small number, the updates of ω_r in consecutive iterations are large and usually nonmonotone. This one, in addition to the known features of the Newton-Raphson method when applied to the time-periodic models regarding a problematic convergence [13], makes the iterative process unstable. For that reason, in the solution of the current problem the Newton-Raphson method will be replaced by the fixed-point technique [13, 14]. The discretized physical equation of mechanical balance (12) will be substituted by the artificial equation of the form:

$$\omega_{r1}\rho_{Fp} - T_{e1}([\varphi_1],[\lambda_1]) = r_{Fp1} \quad \text{for} \quad k = 1, \tag{15a}$$

$$\omega_{rk}\rho_{Fp} - T_{ek}([\varphi_k],[\lambda_k]) = r_{Fpk} \quad \text{for} \quad k = 2,\ldots,m, \tag{15b}$$

where r_{Fp} is the fixed-point residual given by:

$$r_{Fp1} = \omega_{r1}\rho_{Fp} - \left(\frac{I}{\Delta t} + k_f\right)\omega_{r1} + \frac{I}{\Delta t}q_{\omega_r}\omega_{rm} - T_{l0} \quad \text{for} \quad k = 1, \tag{16a}$$

$$r_{Fpk} = \omega_{rk}\rho_{Fp} - \left(\frac{I}{\Delta t} + k_f\right)\omega_{rk} + \frac{I}{\Delta t}\omega_{r(k-1)} - T_{l(k-1)} \quad \text{for} \quad k = 2,\ldots m \tag{16b}$$

and ρ_{Fp} is the fixed-point coefficient being constant during the iterative process [13, 14]. By proper selection of ρ_{Fp} the rise of ω_r from one iteration to another may be slowed down to the extent which provides the convergence at the price of reducing its rate. The condition for the stability of the fixed-point of Equations (15) requires from the derivative of the right-hand side to be less than the unity, and consequently:

$$\rho_{Fp} > \left|\frac{\partial T_{ek}}{\partial_{\omega_{rk}}}\right|, \tag{17}$$

but this derivative is never known in advance. A more practical choice for ρ_{Fp} can be based on the value of $I/\Delta t$. Useful values of ρ_{Fp} are a few (5 to 10) times larger than $I/\Delta t$, but it should be regarded that too high values lead to a loss of contraction and stagnation of the iterative process. In this approach the remaining equations will be solved via the successive approximation with relaxation such that:

$$X_{j+1} = (1-\beta)X_j + \beta\overline{X}_j, \tag{18}$$

where $X = [x_1, x_2, ..., x_{m-1}, x_m]$T, j is the index of the nonlinear iteration, β the relaxation factor, and $\overline{X}$ denotes current solution of (8) considering (15). Figure 2 depicts a flowchart diagram for this algorithm.

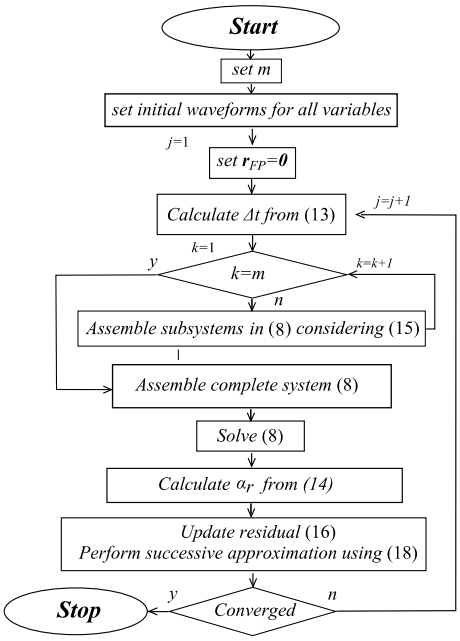

Fig. 2. Flowchart diagram illustrating the algorithm of computations with time-varying rotor speed (prescribed load torque)

3. Computations

3.1. Basic assumptions and reference motors

The calculations are carried out for the two permanent-magnet BLDC motors with specifications summarized in Table 1.

Table 1. Specifications of sample PM-BLDC motors

Parameter	Motor 1 (low-speed motor)	Motor 2 (high-speed motor)
Rated power	180 W	180 W
Rated speed	170 rpm	4000 rpm
Number of pole-pairs	7	2
Rated current	10 A	8 A
Rated DC voltage	24 V	36 V
Winding type	Three-phase, distributed, one-layer, fully-pitched	Three-phase, concentrated, one-layer

Number of turns per coil	18	25
Phase resistance	0.188 Ω	0.25 Ω
Phase end-winding leakage inductance	0.065 mH	0.012 mH
Axial length	40 mm	80 mm
Commutation mode	120°	120°
Skew angle	one slot-pitch	none
Friction coefficient k_f	0.001 N·m·s	0.0005 N·m·s
Moment of inertia J	0.00133 kg · m^2	0.000028 kg · m^2
Permanent magnets	Neodymium, B_r = 1.1 T, H_c = – 950 kA/m	Ceramic, B_r = 0.43 T, H_c = – 191 kA/m

Figure 3 displays basic dimensions of the motors' magnetic circuits, the magnetization characteristics of core parts as well as the static characteristic of parallel diodes used in the functional network model of the voltage source inverter in Figure 1b.

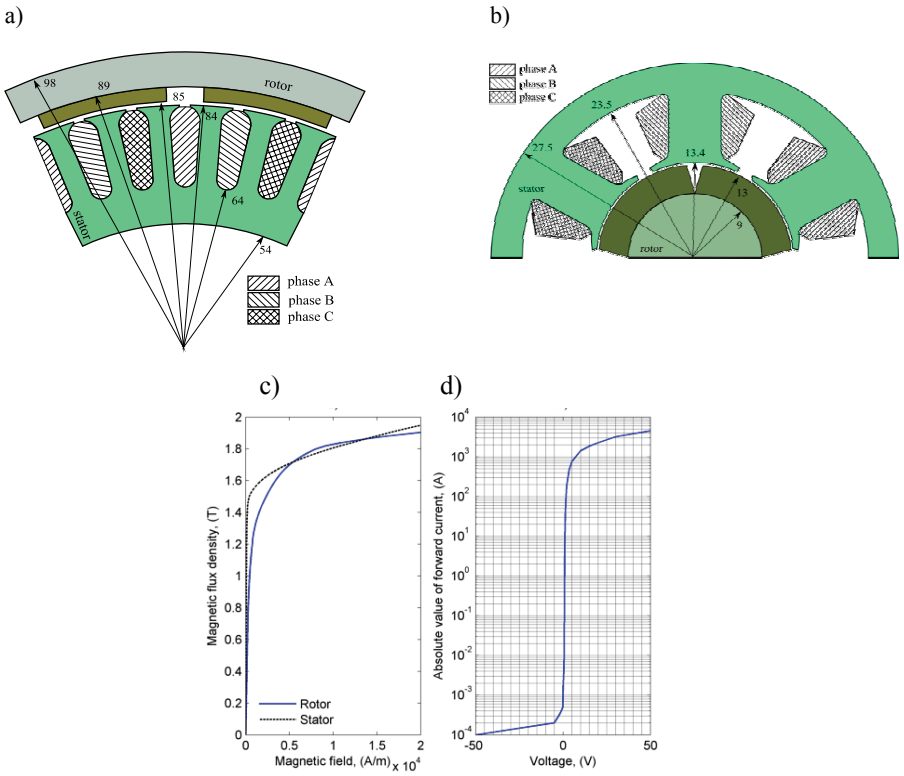

Fig. 3. Models used: a) motor 1, b) motor 2 (one pair of poles considered with positive periodicity conditions), c) magnetization characteristics of motor core parts, d) static characteristic of the parallel diodes of the voltage source inverter

For each out of the two computational cases considered further, the finite element models are built using the positive spatial periodic symmetry condition with respect to one pair of poles, and the half period time-periodic conditions. The relative error tolerance in the non-linear process was set to 10^{-4}. The computations were executed on a PC with a six-core Phenom CPU and 16 GB of memory.

3.2. Computations using model with prescribed rotor speed and unknown load torque

In the first case, the time-periodic model with a prescribed rotor speed is compared with the transient model with respect to execution times. The computations are carried out at the nominal speed. Assuming a constant time-step Δt the resolution of waveforms that guarantees correct representation of all time-harmonics ("spiky" waveforms of phase voltages) is 200. In a time-periodic model the number of steps m is equal to 100 using the half-period time periodicity conditions, which is a sufficient discretisation level to handle the specific voltage waveform in the considered machines. The steady-state in the transient model is understood so as to take place when the waveform of the phase current agrees to within one per cent with that obtained from the time-periodic model, and this is reached here within three and four fundamental periods for Motor 1 and Motor 2, respectively.

The computations for Motor 1 are carried out for models using an increasing number of mesh slices (see Fig. 4a). The results are summarized in Table 2. For this motor, the sufficient number of mesh slices is five. By comparison of execution times, it can be noticed that the time-harmonic model outperforms the transient model until the number of mesh slices is less than nine. For the number of mesh slices equal to five the steady-state solution is achieved in sixty-five per cent of time required by the transient model. This is a satisfactory result, especially as it is clear from the table that the convergence of the-time periodic model is definitely worse than that of the transient model. From the results it can also be deduced that the computational scale of the elaborated time-periodic model is $O(n^2 \cdot \log n)$ with n being the number of unknowns (see Fig 4c). By comparison with that of the time-stepping model, which is clearly $O(n)$, it can be deduced that the time-periodic model has a chance to be competitive to the transient model only up to certain number of unknowns, which corresponds here to seven mesh slices taken into account. It is worth noticing that this performance is possible thanks to specific construction of the solver, which besides internal parallelisation, takes benefits from the matrix structure in the case of the multi mesh-slice model (lack of the off-diagonal blocks in the system matrix due to neglecting of the axial flux). However, as with every direct solver, its performance strongly depends on the matrix size. Therefore, for the models with significantly increased (doubled or tripled) mesh density in a single mesh-slice, the effect in Fig. 4 will be seen for fewer mesh slices.

It should also be noticed, looking at the results in Table 3 that regard motor 2, that the steady-state model is most advantageous in the case of the motor without skew and with a larger electric time-constant, for which the steady-state solution is achieved in less than twenty-five per cent of the time required by the transient model.

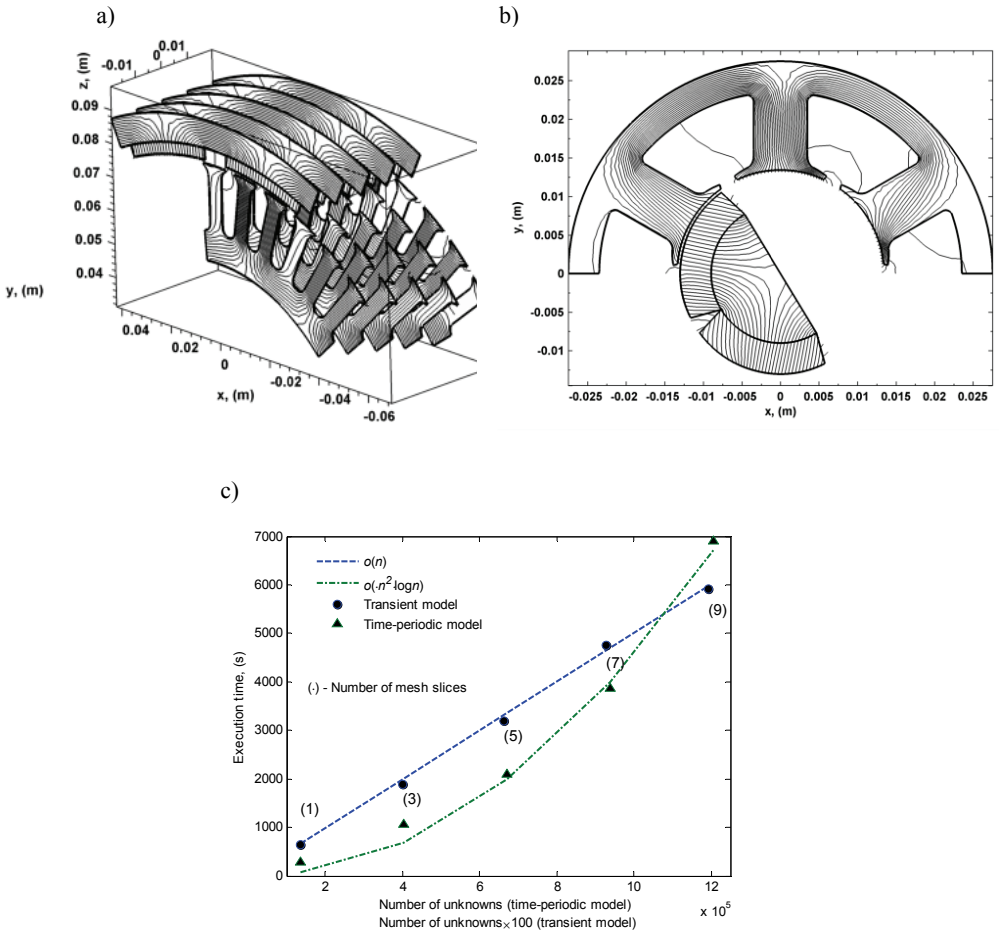

Fig. 4. Results obtained: a) distribution of magnetic flux at the given instant of time for both motors conisidered, b) estimation of computational cost vs. the number of unknowns for the time-periodic and transient models

Table 2. Comparison of total execution times for motor 1, for models with prescribed rotor speed equal to 170 rpm

Number of mesh-slices	**Transient model (three fundamental periods considered)**			**Half-period time-periodic model (100 time-steps considered)**		
	Number of unknowns	Execution time [s]	Average number of iterations per time-step	Number of unknowns	Execution time [s]	Number of iterations
1	1347	650	23	136 047	285	36
3	3995	1880	26	403 495	1064	47
5	6643	3188	27	670 943	2101	54
7	9291	4749	27	938 391	3877	62
9	11 939	5905	31	1 205 839	6914	74

Table 3. Comparison of total execution times for motor 2, for models with prescribed rotor speed equal to 4000 rpm

Transient model (four fundamental periods considered)			**Half-period time-periodic model (100 time-steps considered)**		
Number of unknowns	Execution time [s]	Average number of iterations per time-step	Number of unknowns	Execution time [s]	Number of iterations
2193	3491	28	250480	702	43

3.3. Computations using model with prescribed load torque and unknown speed

In this case the nonlinear problem in the time-periodic model is solved according to the algorithm depicted in Figure 2. Only motor 1 is considered as it is not expected for the motor 2 model to deliver significantly different interpretations.

The motor is considered loaded by the constant rated torque $T_l = 10$ N·m, and the iterations are started from the rotational speed equal to 100 rpm being the central point on the mechanical characteristic. For this initial speed, the ratio $I/\Delta t$ in the first iteration (calculated from data in Table 1 and (13)) is equal to 1.55 N·m·s. The fixed point constant ρ_{Fp} was assumed to be ten times greater. Table 4 summarizes execution times of the model using increasing number of mesh slices, whilst Figure 5 displays the half period waveforms obtained from the time-periodic models as well as those taken from the physical model at this point of operation, that were measured under constant load torque rather than under constant speed. For comparison, the waveforms obtained from the model with forced speed, are dispayed. It can be seen that the electromagnetic torque, current and voltage waveforms are slightly affected by a relatively small speed variation. It should be noticed that the external moment of inertia was assumed to be equal to zero, whilst in physical system it would be increased, and thus the speed variation would be reduced.

From the results in Table 4 it is clear that even though the number of unknowns increased only slightly, the time of computations is two times greater than that in Table 2 for the number of mesh slices equal to five, and this might be considered disappointing. However, noticing that the machine operation point was found here in a single computation, which normally would require at least a few steps with the time-stepping model executed at different rotational speeds, it can be considered as a satisfactory achievement.

Table 4. Comparison of execution times of time-periodic model with unknown time-varying speed for various numbers of mesh slices used. Iterative process is started from rotational speed equal to 100 rpm

Number of mesh slices	**Transient model (600 time-steps considered)**			**Half-period time-periodic model (100 time-steps considered)**		
	Number of unkowns	Execution time [s]	Average number of iterations per time-step	Number of unknowns	Execution time [s]	Number of iterations
1	1349	669	24	136148	336	54
3	3997	1816	28	403596	2116	63
5	6645	2735	35	671044	4415	68
7	9293	4151	46	938492	7777	73
9	11941	5414	49	1205940	15806	83

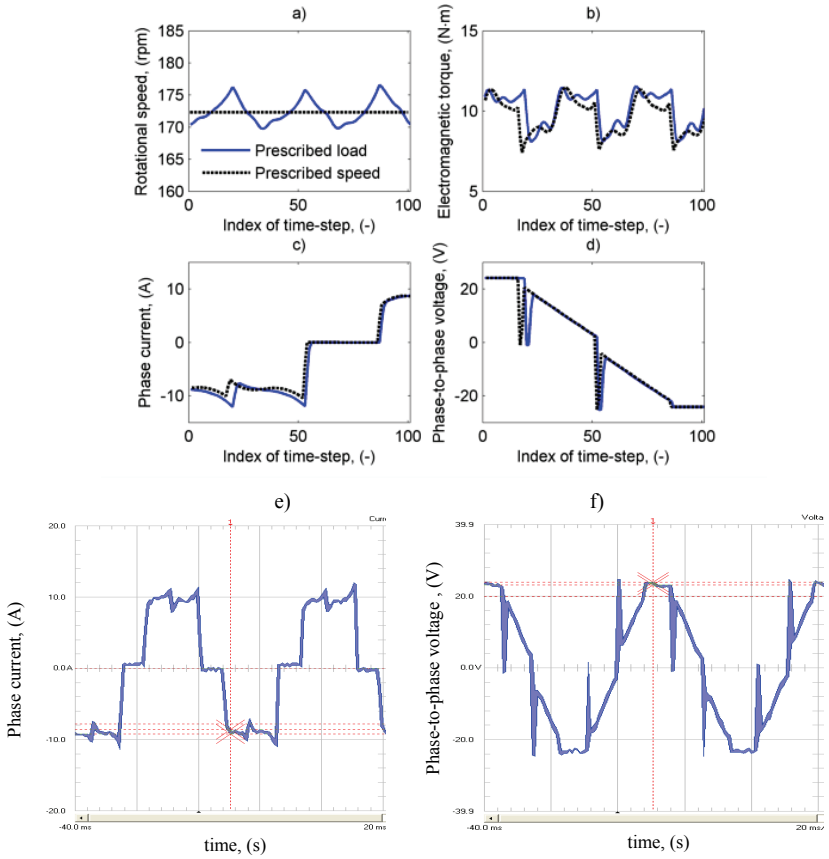

Fig. 5. Computed and measured waveforms: a, b, c, d) computed rotational speed, electromagnetic torque, phase current and phase-to-phase voltage half-period waveforms, e, f) measured waveform of phase current and phase-to phase voltage. Prescribed constant speed is equal to average value of the waveform in Fig. a)

It should be noticed that the comparison of execution time of this model with that of the transient model with the equation of mechanical balance taken into account, would not be a good measure of its performance. This is because the significant part of I is usually imposed by the load and so, it would always be possible to apply such type of loading for which the mechanical time-constant would be high enough.

When running the model, the starting point regarding the rotational speed (100 rpm) was set quite arbitrarily. However, as in every iterative process, a choice of the starting point strongly impacts the performance of the algorithm. With a more accurate estimation of the starting value of angular speed for the given load one should expect shorter execution times of the model. This is presented in Table 5 which summarizes the execution times of the model with five mesh slices for various values of the rotational speeds at the starting point. In this case the average speed at the operation point is equal to 172.3 rpm (see Fig. 5a) and it is apparent that the better the estimate used the shorter the execution time obtained.

Table 5. Comparison of execution times of time-periodic model with five mesh slices considered with respect to rotational speed used as a starting point in nonlinear process. The average rotational speed at this point of operation is equal to 172.3 rpm

Constant rotational speed at initial point in nonlinear iterations [rpm]	**Execution time [s]**	**Number of iterations**
100	4415	68
135	4031	62
170	3327	51
205	5424	83
240	–	not converged within the given iteration limit

In this example the starting point coresponding with 240 rpm results in a very large number of iterations. At the 150th iteration the relative error was still over 10^{-3} and the process was interrupted as it was not converging. At this starting point the motor operates in regenerative braking mode returning energy through parallel diodes. The observed very slow convergence relates to the continuous operation of diode elements. For the remaining starting points the model has converged within the given iteration limit and these results show how important it is to use close estimates of the starting point in this type of model as long as it has to be practical [14]. However, if the permanent-magnet brushless machines are considered, the rotational speed at a given point can be estimated well using even the basic equations of a DC machine and the lumped parameters obtained from simple magnetostatic computations. Obtaining such an estimate will always guarantee a much shorter execution time than in case when the iterative process is started from an arbitrary point.

4. Conclusion

A time-periodic finite element model of a BLDC motor as well as its numerical features have been presented in this work. Use of two methods for considering mechanical motion in this type of model has been compared and discussed for two different motors. It has been shown that the unstable solution obtained when the rotational speed is determined from the auxilary equation of the mechanical balance can be avoided by application of the fixed-point technique. In spite of a computatially massive nature of the time-periodic models, from the point of view of determination of the machine operation point, the model has been shown to be competitive, with respect to the execution time, to the transient model. The main advantage of this approach is providing all of the waveforms in the unique framework allowing for evaluation of not only the machine characteristic, but also the power losses. This can be useful in e.g. thermal analysis of electrical machines using a steady-state static thermal model coupled with the steady-state time-periodic electromagnetic model.

Acknowledgment
Janusz Gwozdz is a beneficiary of the Opole Voivodeship Ph.D. Students Support Programme II, co-funded by The European Social Fund

References

[1] Ashtiani C.N., Lowther D.A., *The use of finite elements in the simulation of steady state operation of a synchronous generator with a known terminal loading condition*. IEEE Trans. Magn. 19(6): 2381-2384 (1983).

[2] Zhou P., McDermott, Cendes Z.J., Rahman M.A., *Steady-state analysis of synchronous generator by a coupled field-circuit method.* Rec. of International Electric Machines and Drives Conference, 18-21 may, Milwakee, USA. pp. WC2/2.1-WC2/2.3 (1997).

[3] Kurihara K., Wakui G., Kubota T., *Steady-state performance analysis of permanent magnet syn chronous motor including space harmonics.* IEEE Trans. Magn. 30(3): 1306-1315 (1994).

[4] Li S.H., *Numerically efficient steady-state finite element analysis of magnetically saturated electro-mechanical devices.* IEEE Trans. Magn. 39(6): 3481-3485 (2003).

[5] Gonzales A., Hernandez C., Arjona-Lopez M., *A 2D-Fe magnetostatic model of a PMSG for predicting its steady-state performance under different loading conditions.* IET Electric Power Applications 7(3): 207-213 (2013).

[6] Yamada S., Bessho K., Lu J., *Harmonic balance finite element method applied to nonlinear AC magnetic analysis.* IEEE Trans. Magn. 25(4): 2971-2973 (1989).

[7] Gyselinck J., Dular P., Vandevelde L. et al., *Two-dimensional harmonic balance finite element modeling of electrical machines taking motion into account.* Int. Journ. Math. Electr. Electron. Eng. COMPEL 22(4): 1021-1036 (2003).

[8] Hara T., Naito T., Umoto J., *Field analysis of corona shield region in high voltage rotating machines by time-periodic finite element mehod.* Journal of IEE Japan 102B(7): 423-430 (1982).

[9] Nakata T., Takahashi N., Fujiwara K., Ahagon A., *3-D non-linear eddy current analysis using the time-periodic finite element method*. IEEE Trans. Magn. 25(5): 4150-4152 (1989).

[10] Nakata T., Takahashi N., Fujiwara K. *Practical analysis of 3-D dynamic nonlinear magnetic field using time periodic finite element method.* IEEE Trans. Magn. 31(3): 1416-1419 (1995).

[11] Takahashi Y., Kaimori H., Kameari A. et al., *Convergence acceleration in steady state analysis of synchronous machines using time-periodic explicit error correction method.* IEEE Trans. Magn. 47(5): 1422-1425 (2011).

[12] Takahashi Y., Tokumatsu T., Fujita M. et al., *Time-domain parallel finite element method for fast magnetic field analysis of induction motors.* IEEE Trans. Magn. 49(5): 2413-2416 (2013).

[13] Peterson W., *Fixed-point technique in computing nonlinear eddy current problems.* Int. Journ. Math. Electr. Electron. Eng. COMPEL 22(2): 231-252 (2003).

[14] Biró O., Koczka G., Leber G. et al., *Finite element analysis of three-phase three-limb power transformer under DC bias.* IEEE Trans. Magn. 50(2): 7013904 (2014).

[15] Plexim GMbH, *Piecewise-Linear Electric Circuit Simulator (PLECS), Documentation/Manual.* www.plexim.com/download/documentation, Accessed May (2014).

[16] Jagiela M., Gwóźdź J., Garbiec T., *Time-periodic steady-state finite element model of inverter driven rotating machine.* Proc. of XXIII Int. Symp. Electromagnetic Phenomena in Nonlinear Circuits, 2-4 July, Plsen, Czech Republic (2014).

[17] Davis T.A., *Algorithm 832: UMFPACK, an unsymmetric-pattern multifrontal method*. ACM Transactions on Mathematical Software 30(2): 196-199 (2004).

[18] Dziwniel P., Boualem B., Piriou F. et al., *Comparison between two approaches to model induction machines with skewed slots.* IEEE Trans. Magn. 36(4): 1453-1457 (2000).

[19] Oliveira A.M., Antunes R., Kuo-Peng P., Sadowski N., Dular P., *Electrical machine analysis considering field-circuit-movement and skewing effect.* Int. Journ. Math. Electr. Electron. Eng. COMPEL 23(4): 357-360 (2004).

[20] Demenko A., Wojciechowski R.M., Sykulski J.K., *On the equivalence of finite element and finite integration formulations*. IEEE Trans. Magn. 46(8): 3169-3172 (2010).

[21] Demenko A., Łyskawinski W., Wojciechowski R.M., *Equivalent formulas for global magnetic force calculation from finite element solution.* IEEE Trans. Magn. 48(2): 195-198 (2012).